ELSEVIER

Journal of Hydrology 222 (1999) 165–184

Journal of Hydrology

Numerical and experimental study of seepage in unconfined aquifers with a periodic boundary condition

B. Ataie-Ashtiani[a,*], R.E. Volker[b], D.A. Lockington[b]

[a]*Department of Civil Engineering, Sharif University of Technology, Tehran, Iran*
[b]*Department of Civil Engineering, University of Queensland, Queensland 4072, Australia*

Received 29 January 1999; received in revised form 11 June 1999; accepted 6 July 1999

Abstract

The assessment of groundwater conditions within an unconfined aquifer with a periodic boundary condition is of interest in many hydrological and environmental problems. A two-dimensional numerical model for density dependent variably saturated groundwater flow, SUTRA (Voss, C.I., 1984. SUTRA: a finite element simulation model for saturated–unsaturated, fluid-density dependent ground-water flow with energy transport or chemically reactive single species solute transport. US Geological Survey, National Center, Reston, VA) is modified in order to be able to simulate the groundwater flow in unconfined aquifers affected by a periodic boundary condition. The basic flow equation is changed from pressure-form to mixed-form. The model is also adjusted to handle a seepage-face boundary condition. Experiments are conducted to provide data for the groundwater response to the periodic boundary condition for aquifers with both vertical and sloping faces. The performance of the numerical model is assessed using those data. The results of pressure- and mixed-form approximations are compared and the improvement achieved through the mixed-form of the equation is demonstrated. The ability of the numerical model to simulate the water table and seepage-face is tested by modelling some published experimental data. Finally the numerical model is successfully verified against present experimental results to confirm its ability to simulate complex boundary conditions like the periodic head and the seepage-face boundary condition on the sloping face.

Keywords: Variably saturated flow; Groundwater flow; Unconfined aquifer; Periodic boundary condition; Finite element model; Flow tank

1. Introduction

Groundwater flow and contaminant migration studies in unconfined coastal aquifers are highly complex, because in addition to other difficulties these aquifers are prone to sea water intrusion which complicates the flow pattern near the sea boundary. Also, the presence of the coastal boundary of the aquifer makes the problem more complex because tidal fluctuations and the mild slope of beaches can cause a long seepage-face to develop in the beach. The capillary fringe may also have a significant effect on water level position when there are tidal fluctuations.

Approximate analytical solutions of the one-dimensional (1D) Boussinesq equation for the groundwater behaviour in response to tidal fluctuations have been presented by several authors (Philip, 1973; Smiles and Stokes, 1976; Nielsen, 1990). In these solutions, it is assumed that decoupling between the water table and

* Corresponding author. Faculty of Civil Engineering, Delft University of Technology, P.O. Box 5048, 2600 Delft GA, Netherlands. Fax: + 31-15-278-5915.

E-mail address: b.ataie@ct.tudelft.nl (B. Ataie-Ashtiani)

0022-1694/99/$ - see front matter
PII: S0022-1694(99)00105-5

the tide does not occur. In cases with tidal fluctuations this assumption is probably too simple, as during the ebb period the exit point is often decoupled from the sea level and a seepage-face is formed (Nielsen, 1990). Although analytical solutions are simple and instructive for those cases where decoupling does not occur, they are not adequate for predicting the behaviour of a dynamic exit point and seepage-face and, therefore, for predicting the full water table and groundwater dynamics. Analytical models are also limited by assuming: a uniform thickness of aquifer above an impermeable layer underlying the beach; a constant beach face angle; a uniform hydraulic conductivity and specific yield; and a single inland boundary condition at which water table oscillations reduce to zero. Moreover all the analytical solutions are based on the assumption that the water in the aquifer is a single-phase homogenous fluid. Therefore, to overcome these limitations, numerical methods need to be applied.

Fang et al. (1972) simulate the tidal fluctuation of the groundwater table, numerically, by using a two-dimensional (2D) finite element model. Flow was considered in a simplified domain with a vertical beach face. Li et al. (1997) present a numerical model based on the boundary element method, which simulates 2D groundwater flow with free and moving boundary conditions, including the seepage dynamics at the beach face. This model is limited to a fully saturated and homogeneous flow domain.

Several numerical models are available for simulating the movement of water in variably saturated porous media (e.g. Rubin, 1968; Cooley, 1971; Kirkland et al., 1992). Among them, only a few can simulate groundwater flow in unconfined aquifers with complex boundary condition like a seepage-face (e.g. Cooley, 1983; Clement et al., 1994) and even fewer can also consider sloping or irregular boundaries that are quite common at most hydrogeological interfaces (e.g. Neuman, 1973; Huyakorn et al., 1984). To the authors' knowledge, none of the variably saturated models has been applied for numerical simulation of groundwater behaviour in an unconfined aquifer in response to a periodic boundary condition on a sloping face of an aquifer. Moreover, to model the effects of tidal fluctuations on sea-water intrusion in coastal aquifers, the model also should be able to simulate density dependent groundwater flow.

This paper reports the details of necessary modifications and verifications of a numerical model for simulation of groundwater flow in unconfined aquifers affected by periodic boundary conditions. This study has three objectives. The first is to improve one of the available 2D finite element models for density dependent variably saturated flow so that it can simulate groundwater flow in an unconfined aquifer with a sloping face on which is imposed a periodic boundary condition. The second is to provide physically measured results for the groundwater response to the periodic boundary condition for aquifers with both vertical and sloping faces. The final objective is to verify the modified numerical model by duplicating experimental data both published and obtained during this study. The modified numerical model is used to investigate the effects of tidal fluctuations on groundwater hydraulics, sea-water intrusion and contaminant transport in unconfined aquifers (Volker et al., 1997; Ataie-Ashtiani et al., 1999a,b).

2. Numerical model

SUTRA (Voss, 1984) was chosen as the basis for numerical modelling because of its ability to solve density dependent groundwater flow and variably saturated flow, and also because it is readily available in source code form.

This model implements a hybridisation of finite element and integrated finite difference methods employed in the framework of a method of weighted residuals. In this model, standard finite element approximations are employed only for terms in the balance equations that describe fluxes of fluid mass, solute mass and energy. All other non-flux terms are approximated with a finite element mesh version of the integrated finite difference methods. The hybrid method is the simplest and most economical approach which preserves the mathematical elegance and geometric flexibility of finite element simulation, while taking advantage of finite difference efficiency. The finite element method allows the simulation of irregular regions with irregular internal discretisation. This is made possible through use of quadrilateral elements with four corner nodes (Voss, 1984).

SUTRA was primarily intended for simulation of 2D flow, and either solute or energy transport in

saturated variable-density systems, while unsaturated flow and transport processes were included to allow simulation of some unsaturated problems. Voss (1984) mentioned that SUTRA numerical algorithms were not customised for the non-linearity of unsaturated flow as would be required of a model simulating only unsaturated flow. He also states that SUTRA requires fine spatial and temporal discretisation for unsaturated flow, and is therefore not an economical tool for extensive unsaturated flow modelling. Therefore this model has not been extensively used for variably saturated problems.

In the present work SUTRA has the following advantages:

1. Spatial approximation of the variably saturated flow equation using the hybrid finite element and finite difference method is naturally mass lumping, in contrast to common formulations of the finite-element method, which require mass lumping to avoid oscillatory solutions (Celia et al., 1990).
2. The hybrid finite element and finite difference method has all the abilities of finite element methods to handle irregular geometries and complex boundary conditions.

In this study, SUTRA has been improved for modelling of groundwater flow and contaminant transport in an unconfined coastal aquifer by three changes. First, in order to enhance the ability of the model for handling variably saturated flow, the basic flow equation is changed from pressure- to a mixed-form of the general 2D variably saturated flow equation. The mixed form is solved using the modified Picard iteration scheme presented by Celia et al. (1990).

Second, to improve the ability of the model to handle the non-linearity of the unsaturated zone equation, an automatic under-relaxation method is applied for adjustment of pressure after each iteration.

Finally, the model has also been adjusted to handle a seepage-face boundary condition which is especially important in the cases where there is a large amplitude tidal fluctuation on mild slope beaches.

2.1. Mathematical formulations

The governing equations describing the SUTRA fluid mass balance, in pressure-based form are (Voss, 1984)

$$\frac{\partial}{\partial x_i}\left[\frac{k_{ij}k_r\rho}{\mu}\left(\frac{\partial p}{\partial x_j}-\rho g e_j\right)\right]=\left(S_w\rho S_{op}+\varepsilon\rho\frac{dS_w}{dp}\right)\frac{\partial p}{\partial t}+\varepsilon S_w\frac{\partial\rho}{\partial c}\frac{\partial c}{\partial t}-Q_p \tag{1}$$

where p is the pressure, c the solute concentration of fluid as a mass fraction, k_{ij} the permeability tensor, k_r the relative permeability with respect to the water phase, x_i $(i=1,2)$ the Cartesian coordinates, t the time, e_j the unit gravitational vector in the direction of x_2 (assumed to be vertically upward), Q_p a fluid mass source, S_w the saturation, S_{op} the specific pressure storativity, ρ the fluid density, μ the fluid viscosity, ε the porosity, and g the gravitational acceleration.

The coefficient of time derivative of the pressure, p, on the right-hand side of Eq. (1) consists of two parts. The first part, $(S_w\rho S_{op})\partial p/\partial t$, represents the effect of specific storage due to changes in pressure. This storage is due to the temporal changes in fluid density and formation porosity. The second part, $(\varepsilon\rho(dS_w/dp))\partial p/\partial t$, describes the effects of draining and filling pores. This term can be written in its simpler form, $\varepsilon\rho(\partial S_w/\partial t)$. Although these expressions are equivalent mathematically in a continuous partial differential equation, the discrete analogies of $\partial S_w/\partial t$ and $(dS_w/dp)\partial p/\partial t$ are not equivalent. This inequality is amplified owing to the highly non-linear nature of the specific capacity term, dS_w/dp. Using the modified Picard approach eliminates this problem by directly approximating the temporal term $(\partial S_w/\partial t)$ with its algebraic analogue (Clement et al., 1994).

In the present work SUTRA has been modified to solve the mixed form of variably saturated flow equation

$$\frac{\partial}{\partial x_i}\left[\frac{k_{ij}k_r\rho}{\mu}\left(\frac{\partial p}{\partial x_j}-\rho g e_j\right)\right]=S_w\rho S_{op}\frac{\partial p}{\partial t}+\varepsilon\rho\frac{dS_w}{dt}+\varepsilon S_w\frac{\partial\rho}{\partial c}\frac{\partial c}{\partial t}-Q_p \tag{2}$$

This mixed form is capable of modelling a wide variety of problems, including infiltration into dry soil. The modified Picard iterative procedure for the

mixed form flow equation is fully mass conserving in the unsaturated zone. By contrast, conventional, pressure-based formulations exhibit poor mass-balance behaviour.

2.2. Numerical methods

The weighted residual numerical method combining Galerkin finite elements with integrated finite differences is applied to approximate Eq. (2). Voss (1984) explains that great geometric flexibility in mesh design is allowed by using the Galerkin finite element method. Also, an integrated finite difference approximation for the spatial integration of all non-flux terms in the governing equations provides an economical alternative to the Galerkin method while maintaining accuracy sufficient for any mildly non-linear simulation problem.

The numerical method for solving the mixed form of variably saturated flow equation including the effect of density variation will now be explained in detail. The same procedure is applied for the solute transport equation and the detail is given in the SUTRA manual (Voss, 1984).

Pressure is discretised as a piecewise continuous function in space using bilinear basis functions on quadrilateral finite elements. This is expressed for a mesh with *NN* nodes as

$$p \approx \sum_{I=1}^{NN} p_I(t)\phi_I \tag{3}$$

where $p_I(t)$ is the value of pressure at node I and ϕ_I is the basis function defined at node I.

Applying a weighted residual method to Eq. (2), results in:

$$\int_A \left[\frac{\partial}{\partial x_i}\left[\frac{k_{ij}k_r\rho}{\mu}\left(\frac{\partial p}{\partial x_j} - \rho g e_j \right) \right] \right]_I \phi_I \, \mathrm{d}A = \int_A \left[S_w \rho S_{op} \frac{\partial p}{\partial t} + \varepsilon \rho \frac{\partial S_w}{\partial t} \right]_I \phi_I \, \mathrm{d}A + \int_A \left[\varepsilon S_w \frac{\partial \rho}{\partial c}\frac{\partial c}{\partial t} \right]_I \phi_I \, \mathrm{d}A - \int_A [q]_I \phi_I \, \mathrm{d}A \tag{4}$$

where A is area. An integrated finite difference technique for the time derivative and source term may be implemented by assuming that the complete term involving the time derivative and the source has a constant value throughout a cell surrounding the node. The cell extends to the boundary defined by the connected bisector of opposite sides of all elements contiguous to a node. The area of the cell at node I, A_I, is given by

$$A_I = \int_A \phi_I \, \mathrm{d}A \tag{5}$$

By clearing the integrals of constants, applying Green's theorem, the weighted residual relation becomes

$$AF1_I\left(\frac{\mathrm{d}p}{\mathrm{d}t} \right)_I + AF2_I\left(\frac{\partial S_w}{\partial t} \right)_I + \sum_{J=1}^{NN} BF_{IJ}p_J + CF_I\left(\frac{\mathrm{d}c}{\mathrm{d}t} \right)_I - DF_I - Q_I - Q_{IN\,I} = 0 \tag{6}$$

where:

$$AF1_I = (S_w S_{op})_I A_I \tag{7a}$$

$$AF2_I = \varepsilon \rho A_I \tag{7b}$$

$$BF_{IJ} = \int_A \left\{ \left[k_{ij}^L \left(\frac{k_r \rho}{\mu} \right) \right] \nabla \phi_J \right\} \nabla \phi_I \, \mathrm{d}A \tag{7c}$$

$$CF_I = \left(\varepsilon S_w \frac{\partial \rho}{\partial c} \right)_I A_I \tag{7d}$$

$$DF_I = \int_A -\left\{ k_{ij}^L \left(\frac{k_r \rho}{\mu} \right) \rho g e_j \right\} \nabla \phi_I \, \mathrm{d}A \tag{7e}$$

$$Q_I = qA_I \tag{7f}$$

$$Q_{IN\,I} = \int_B V_n \phi_I \, \mathrm{d}A \tag{7g}$$

where k_{ij}^L indicates an elementwise discretised permeability tensor, V_n the normal Darcy flux intensity at the boundary, and B is the domain boundary. The term $(k_r\rho/\mu)$ is discretised based on nodewise values of p and c. In DF_I, ρg is discretised in a way to be consistent with the discretisation of ∇p (Voss, 1984).

Temporal variations in storage owing to changes in pressure are approximated using backward finite

differences. For the first part we have

$$AF1_I\left(\frac{\mathrm{d}p}{\mathrm{d}t}\right)_I \approx AF1_I\left(\frac{p^{n+1,m+1}-p^n}{\Delta t}\right)_I \tag{8}$$

where the superscript n indicates the time iteration; and Δt is the time step.

A backward Euler approximation, coupled with a Picard iteration scheme, is used to discretise the second term of the left side of Eq. (6), containing the time derivative of the water saturation:

$$AF2_I\left(\frac{\partial S_\mathrm{w}}{\partial t}\right)_I = AF2_I\left(\frac{S_\mathrm{w}^{n+1,m+1}-S_\mathrm{w}^n}{\Delta t}\right)_I \tag{9}$$

After Celia et al. (1990), $S_\mathrm{w}^{n+1,m+1}$ is expanded using a first-order, truncated Taylor series, in terms of the pressure-head perturbation arising from the Picard iteration, about the expansion point $(S_\mathrm{w}^{n+1,m+1}, p^{n+1,m+1})$, as

$$S_\mathrm{w}^{n+1,m+1} \approx S_\mathrm{w}^{n+1,m} + \left.\frac{\mathrm{d}S_\mathrm{w}}{\mathrm{d}p}\right|^{n+1,m}[p^{n+1,m+1}-p^{n+1,m}] \tag{10}$$

The time derivative of concentration is evaluated using the information from the previous time step, using an explicit scheme. Therefore the solution for pressure at nodes, p_I^{n+1}, at the end of the present time step is found from the following equation:

$$\begin{aligned}\left(\frac{AF1_I^{n+1}}{\Delta t_{n+1}} + \frac{AF2_I^{n+1}}{\Delta t_{n+1}}\left.\frac{\mathrm{d}S_\mathrm{w}}{\mathrm{d}p}\right|^{n+1}\right)p_I^{n+1} + \sum_{J=1}^{NN} p_J^{n+1}BF_{IJ}^{n+1} \\ = Q_I^{n+1} + Q_{IN\,I}^{n+1} + DF_I^{n+1} \\ + \left(\frac{AF1_I^{n+1}}{\Delta t_{n+1}} + \frac{AF2_I^{n+1}}{\Delta t_{n+1}}\left.\frac{\mathrm{d}S_\mathrm{w}}{\mathrm{d}p}\right|^{n+1}\right)p_I^n \\ - \left(\frac{AF1_I^{n+1}}{\Delta t_{n+1}}\right)S_\mathrm{w}^{n+1} - CF_I^{n+1}\left(\frac{\mathrm{d}c}{\mathrm{d}t}\right)_I^n\end{aligned} \tag{11}$$

To enhance the convergence for the cases involving variably saturated flow, updating of nodal pressure values is done by applying an under-relaxation formula of the form

$$p^{n+1,m+1} = (1-\gamma)p^{n+1,m} + \gamma p^{n+1,m+1} \tag{12}$$

where γ is an iteration-dependent relaxation factor. For each iteration the value of γ is determined using an adaptation of the empirical scheme developed by Cooley (1983). Following Huyakorn et al. (1984), in this work the current value of γ is obtained as follows:

$$\gamma = \frac{3+s}{3+|s|} \qquad s \geq -1 \tag{13a}$$

$$\gamma = \frac{1}{2|s|} \qquad s < -1 \tag{13b}$$

where s is an iteration parameter. This parameter is defined as

$$s = 1 \qquad r = 0 \tag{14a}$$

$$s = \frac{ep_{m+1}}{\gamma_\mathrm{old} ep_m} \qquad r > 0 \tag{14b}$$

where γ_old is the old value of γ, and ep_m and ep_{m+1} are the pressure errors that are largest in absolute value for iteration m and $m+1$, respectively.

2.3. Boundary conditions

Specified pressure (Dirichlet), and flux (Neumann) boundaries are handled by the original form of SUTRA. In the course of the present project the seepage-face boundary condition has been added to the model.

A seepage-face is an external boundary of the saturated zone where flux is directed outward and there is atmospheric pressure along that boundary. Negative pressures exist above the seepage-face within the porous medium. Therefore, atmospheric pressure is maintained for all the nodes along the seepage-face and they are treated as Dirichlet nodes with the prescribed pressure, $p = 0$. Nodes above the seepage face are specified as no-flow nodes. The position of the seepage-face is initially unknown and constitutes a non-linear boundary condition. Hence, the seepage-face must be determined using an iterative process. Cooley (1983) modified the Neuman (1973) iterative procedure to determine the seepage-face length. The same procedure is used in this work.

The location of the seepage-face is adjusted at the end of each iteration. The seepage-face is lowered one node each iteration until it is one node below the first node encountered having positive pressure. At the same time, the iterative process is allowed to converge

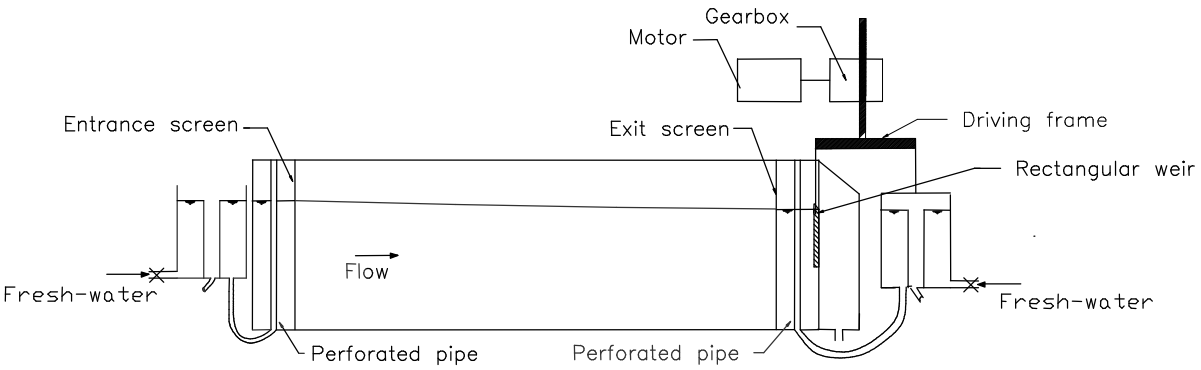

Fig. 1. Layout of the experimental facility.

until the largest absolute error in pressure is less than or equal to 10 times the pressure convergence tolerance. Then the algorithm raises the seepage-face by one node at each iteration until it is at the correct height, as indicated by the node just above the seepage face having negative pressure.

3. Physical model

The layout of the experimental facility is shown in Fig. 1. The apparatus was designed to simulate ground water flow in an unconfined aquifer with a periodic boundary condition at one end.

3.1. Experimental set-up

The experimental apparatus can be subdivided into four major components, the flow tank model, inflow and outflow supply, fluctuator mechanism, and data acquisition system.

3.1.1. Flow tank model

The flow container was made out of a 24 mm thick clear acrylic material. The container consists of two end pieces, two partition pieces or screens, one base piece and two side panels. At one end a special facility was designed to impose a periodical boundary condition. In order to prevent any deformation of

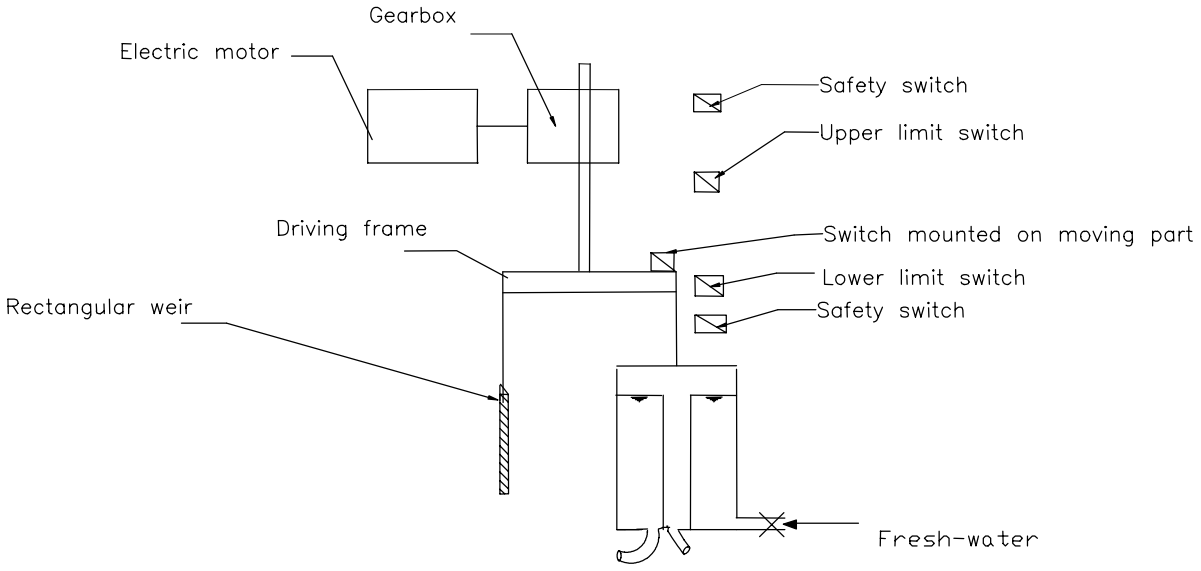

Fig. 2. Fluctuator mechanism.

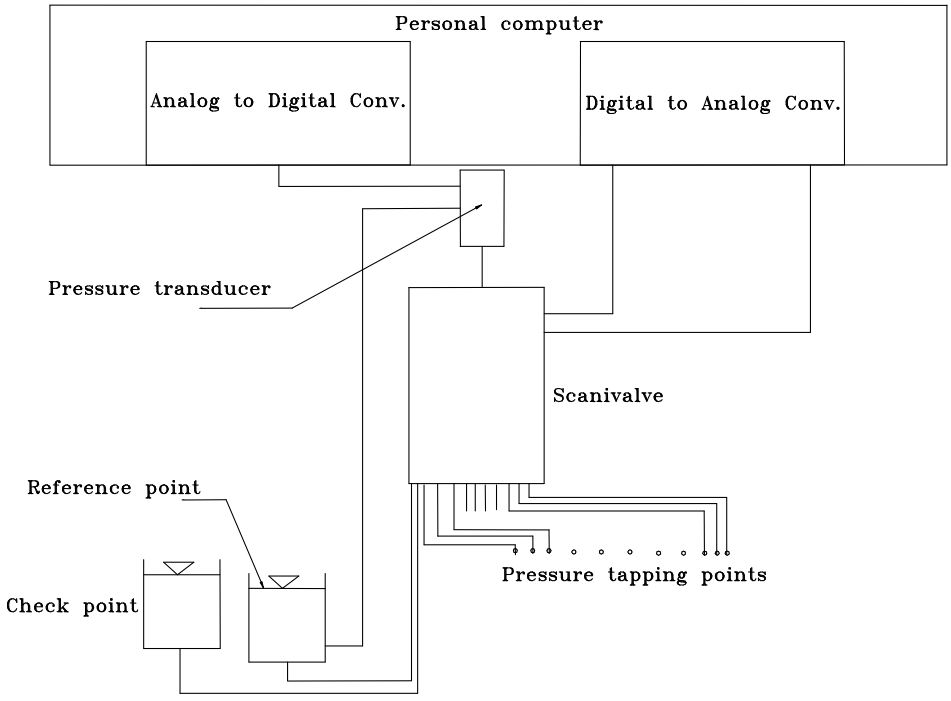

Fig. 3. Data acquisition system.

side walls due to the glass beads and water weight, the side walls were tied to each other by nine 6 mm diameter steel bars. At the back side panel 1 mm holes were made for pressure head measurement. The Plexiglass flow container was supported by a steel frame which was made of 50 mm × 50 mm × 3 mm square tube.

3.1.2. Inflow and outflow water supply

At the up-stream end of the tank, water is supplied from a main supply tap after passing through a filter. To control the entry head of water a constant head tank of 8 l capacity was used. A 40 mm diameter pipe at the middle of the container kept the water level constant. The overflow from this container was directed to the sink, and the remaining flow is supplied at a constant head to a perforated pipe in the end chamber of the sand tank through 30 mm inside diameter (i.d.) vinyl tubing. At the down-stream end, water is supplied from a 450 l reservoir. An electric centrifugal pump delivers water from the reservoir to a constant head tank via 30 mm i.d. flexible vinyl tubing and through a filter.

3.1.3. Fluctuator mechanism

A mechanism was designed to impose a periodic head boundary condition at one end of the tank. Fig. 2 shows a schematic representation of the system. This mechanism produced a linear periodic motion.

A rectangular gate was installed behind the end wall in 8 mm deep grooves in the side walls. This gate was connected to a 50 mm × 50 mm × 3 mm square tube by two rods each 6 mm diameter.

At the other end of the 400 mm long square tube, the constant head container was hung. This container was installed in position so that the top of the overflow pipe was at the same elevation as the top of the rectangular gate. As the container was connected via a vinyl tube of 30 mm i.d. to the downstream chamber of the tank, the water levels in the end chamber and the container were equal.

A 12 V DC motor through a gear box controlled the vertical movement of the whole system of gate and constant water level container together. The speed of the motor was controlled by a variable DC supply. Therefore a different period could be imposed by changing the speed of the motor.

Table 1
Glass beads sieve analysis

Sieve no.	18	20	25	30	35
Diameter (μm)	1000	800	710	600	500
% Passing	99.84	92.6	9.84	0.69	0.03

A circuit was produced to control the motor movement direction. Two micro switches were mounted as the high and low limit of the movement mechanism. These micro switches could be moved to adjust the amplitude of fluctuations. Another switch was mounted as part of the moving mechanism and when this switch reached either of the limit switches the circuit caused the motor direction to be reversed. An additional limit switch was installed for each direction so that the motor power supply would be cut off if a direction control micro-switch failed to operate.

3.1.4. Data acquisition

The data acquisition system was set up similar to that of Demetriou (1990). The system was controlled by a microcomputer through a driver program which controlled the input and output devices. VIEWDAC software was used as the driver program in this work. Pressure readings were taken automatically by specifying the time interval between pressure readings. A time delay was also programmed to occur before each reading so that the pressure reading stabilised before it was logged. Electrical signals for switching and reading different pressure points were passed through the digital to analogue converter (DAC) while the readings were returned to the computer through the analogue to digital converter (ADC). The principal components of the data acquisition system are shown in Fig. 3.

The pressure transducer used for the experiments was a VALIDYNE P305D differential pressure transducer with a 145 mm range. One side of the pressure transducer was connected to the 48 port scanivalve and the other to a water level column to which the pressure readings were referenced.

The water level of the reference point was adjusted prior to the commencement of the experiments to be slightly lower than the lowest water level in the tank at the down-stream end of the flume.

The reference water level of the transducer was connected to the last position of the scanivalve, so that at the end of every cycle of the scanivalve, a zero head difference should be recorded. If this was not observed, it meant that there was a malfunction in the scanivalve-transducer system.

The other check which was implemented was to connect one of the scanivalve ports to a constant head column (not connected to the flume). Since the water level remained unchanged through time, the difference between this water level and the reference point must also remain unchanged.

Before the commencement of the experimental runs, the pressure transducer was calibrated against known head differences and the linear equation relating the transducer output voltage to the head difference was checked. This equation was then incorporated into the computer program which automatically displayed the corresponding head differences measured in millimetre of water.

3.2. Porous medium characteristics

The selected porous medium was composed of very uniform glass beads; the grain size analysis is presented in Table 1.

Glass beads were packed in the flow container as uniformly as possible. They were poured into a 20–30 mm layer of water through a packer box. The water layer was assumed not to cause any size segregation of the glass beads. The packer box, made of five screens with 3 mm openings, is used for uniform distribution of glass beads (Waygal, 1963). Every layer was compacted with a tamper until no further subsidence was noticed.

The porosity n was estimated to be 0.32 by weighing the amount of glass beads (W_s) needed to fill a known tank volume V_0. Knowing the glass beads' particle density ρ_b which was estimated by using a pycnometer to be 2600 kg m^{-3}, n can be obtained from the expression:

$$n = 1 - \frac{W_s}{V_0 \rho_b} \tag{15}$$

The value of the saturated hydraulic conductivity K was determined in situ. For the steady-state flow case, using Darcy's law and the Dupuit–Forchheimer

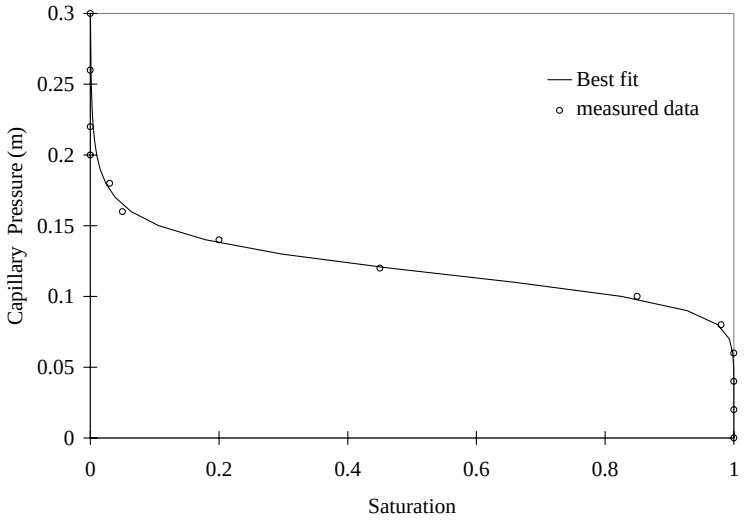

Fig. 4. Glass beads water retention curve.

assumption it can be shown that:

$$K = \frac{Q_x/A_s}{(h_1 - h_2)/L} \tag{16}$$

where Q_x is the discharge rate, L the length of the porous medium along the flow direction and A_s the saturated cross-sectional area. A_s can be expressed as (Oostrom et al., 1992),

$$A_s = Wh_s = W[0.5(h_1 + h_2) + h_c] \tag{17}$$

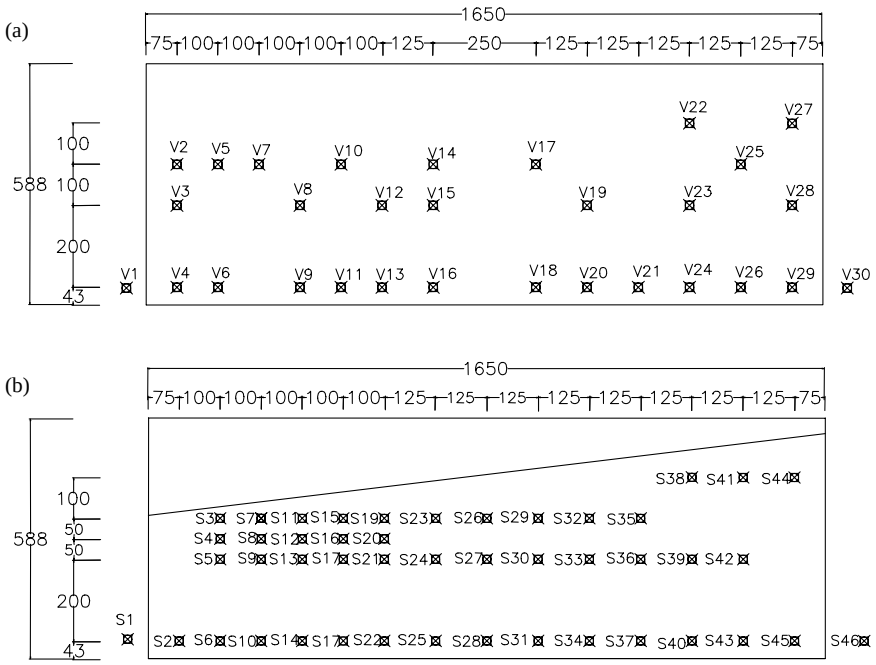

Fig. 5. Position of pressure ports for: (a) vertical; and (b) sloping face cases. (Note: all dimensions in millimetres.)

Table 2
The details of each experiment

Run #	H_{up} (mm)	H_{down} (mm)	Amplitude (mm)	Period (s)	Slope
1	500	483	26	1800	Vertical
2	501	484	28	4900	Vertical
3	500	446.5	62.5	4000	Vertical
4	501	447.5	63.5	10 800	Vertical
5	501	400.5	0	–	1:8.25
6	502	453.5	51.5	3300	1:8.25

where W is the average width of the porous medium, h_s the effective saturated depth, and h_c the height of the capillary fringe. The capillary fringe of the glass beads based on water retention curve was 0.07 m. The average saturated hydraulic conductivity was 15.42 m h^{-1} with values ranging from 15.21 to 15.63 m h^{-1} over six measurements.

The water retention curves of the glass beads were

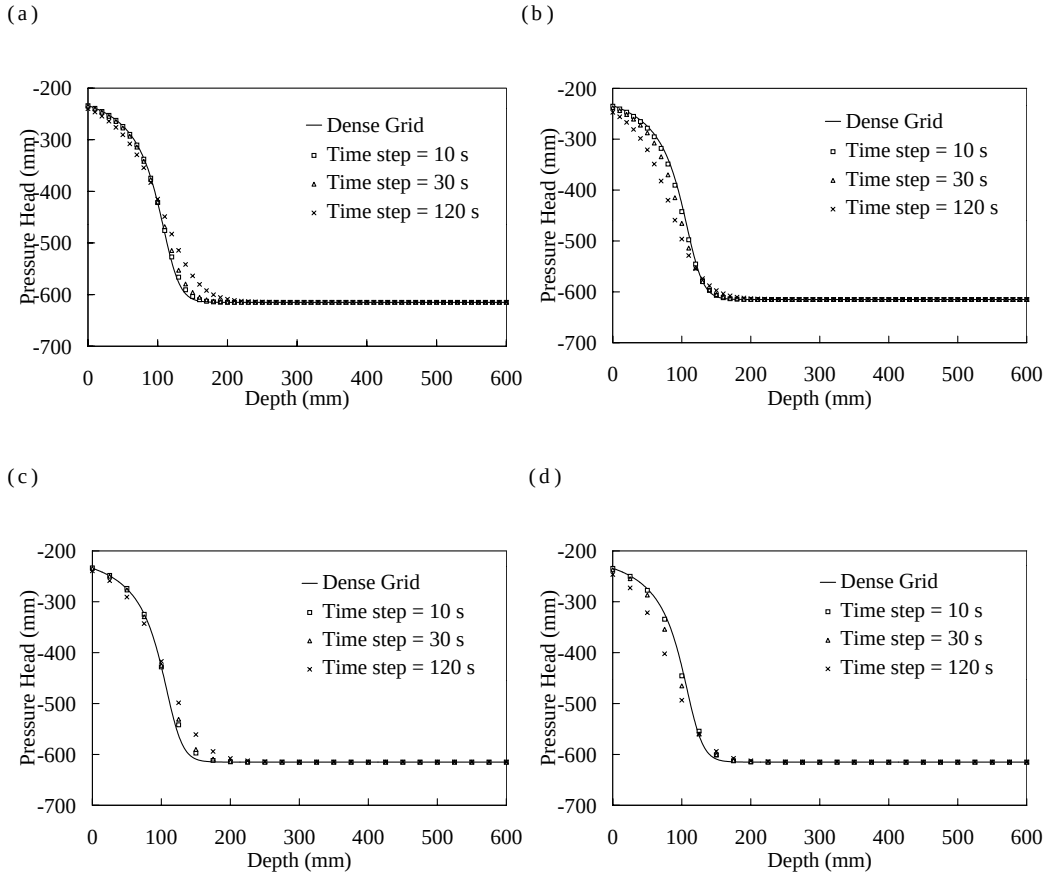

Fig. 6. Comparison between the dense grid solution and coarser mesh solutions: (a) mixed form equation solution with $\Delta y = 10$ mm; (b) pressure-form equation solution with $\Delta y = 10$ mm; (c) mixed-form equation solution with $\Delta y = 25$ mm; (d) pressure-form equation solution with $\Delta y = 25$ mm.

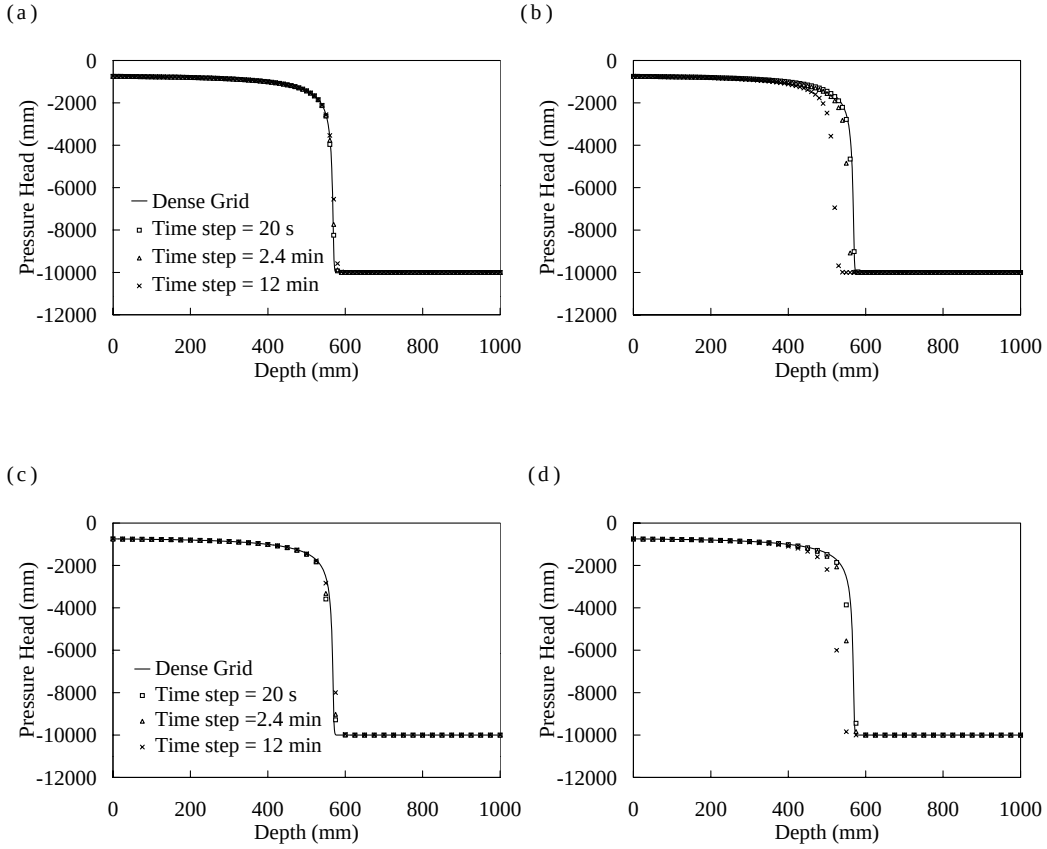

Fig. 7. Comparison between the dense grid solution and coarser mesh solutions: (a) mixed-form equation solution with $\Delta y = 10$ mm; (b) pressure-form equation solution with $\Delta y = 10$ mm; (c) mixed-form equation solution with $\Delta y = 25$ mm; (d) pressure-form equation solution with $\Delta y = 10$ mm.

determined in the laboratory using an apparatus similar to that presented by Van Geel and Sykes (1994). The results are presented in Fig. 4. Using the Levenberg–Marquardt algorithm (Press et al., 1987) and non-linear least-squares regression, the Van Genuchten (1980) model parameters were devised to fit the data. The results are $\alpha = 8.6$ and $n = 9.5$.

Table 3
The values of relative root mean square error (R_{rms}) for Case I

	Δy					
	10 mm			25 mm		
Time step, Δt (s)	10	30	120	10	30	120
Mixed-form equation	0.01	0.02	0.06	0.02	0.03	0.07
Pressure-form equation	0.03	0.07	0.16	0.04	0.07	0.15

Table 4
The values of relative root mean square error (R_{rms}) for Case II

	Δy					
	10 mm			25 mm		
Time step, Δt (s)	20	144	720	20	144	720
Mixed-form equation	0.01	0.06	0.14	0.22	0.18	0.11
Pressure-form equation	0.08	0.61	1.45	0.27	0.51	1.26

3.3. Experimental procedure

The up-stream water level was set by adjusting the position of the constant head container. The down-stream water level and the amplitude of oscillation were set by adjusting the position of upper and lower limit micro-switches. The period of the oscillation was also set by adjusting the input voltage to the electric motor.

The oscillations were initiated more than 12 h prior to the commencement of readings in order to allow the system to reach equilibrium. The pressure at each tapping point was recorded by the data acquisition system for at least five periods of oscillations. These results were considered valid only if they showed that equilibrium had been reached.

The experiments can be divided into two groups. The first group, which consists of four experiments, was conducted for the vertical face configuration. The positions of pressure tapping points for this case are shown in Fig. 5(a). After completion of the experiments for the vertical case, some glass beads were removed very carefully from the top in order to perform the experiments for the sloping case. The surface slope of the packed glass beads in this case was 1:8.25. For the second group of experiments the position of pressure tapping points were changed also and are shown in Fig. 5(b). Table 2 gives the details of each experiment.

The recorded pressures at the different stages of fluctuations at tapping points are given in Ataie-Ashtiani (1998).

4. Numerical results and comparison with experimental data

In this section first the results of the pressure- and mixed-form equation are compared for two 1D problems. Then the numerical model is used to duplicate the results of some published experimental date for variably saturated problems to examine the ability of the model to simulate 2D problems with emphasis on complex boundary condition like seepage-face. Finally the numerical model is verified against the present experimental results.

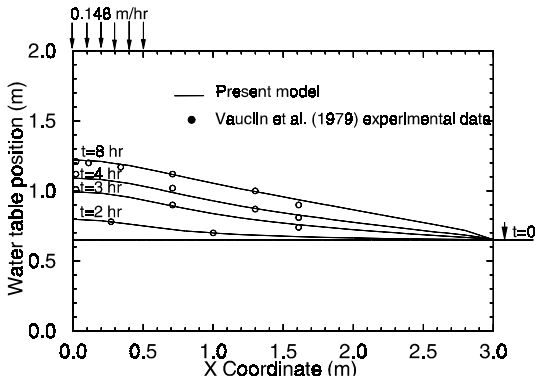

Fig. 8. Comparison of simulated and measured water table for data collected by Vauclin et al. (1979).

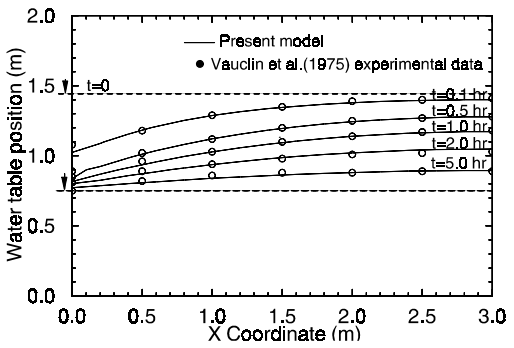

Fig. 9. Comparison of simulated and measured water table for data collected by Vauclin et al. (1975).

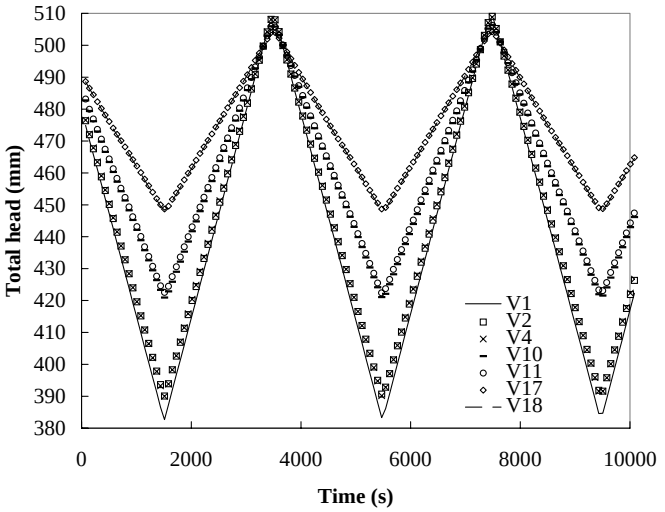

Fig. 10. Total pressure measured at V1, V2, V4, V10, V11, V 17 and V18 for Run #3.

4.1. One-dimensional numerical results

Two 1D problems with different boundary conditions are simulated to compare the results of pressure- and mixed-form approximations. Besides visual comparison of results, the value of the relative root mean square error (R_{rms}) is used in the analysis of accuracy. The definition of R_{rms} is the square root of the average-squared relative deviation of numerical results from the exact solution, at specified spatial reference points at given times. Magnuson et al. (1990) and El-Kadi and Ling (1993) applied this parameter to evaluate how well a numerical model performs. Magnuson et al. (1990) proposed that the values of R_{rms} in the ranges, less than 0.01, from 0.01 to 0.05, and from 0.05 to 0.10 show, respectively, excellent, good, and acceptable accuracy of the numerical model results.

4.1.1. Case I: infiltration in a vertical soil column with flux boundary condition

As the first example, a constant flux infiltration into a vertical column of sand of 600 mm length is simulated (Haverkamp et al., 1977). A constant flux of 136.9 mm h^{-1} at the top of the column and a constant pressure head of -615 mm at the bottom are imposed as boundary conditions and a uniform pressure head of -615 mm is considered as the initial condition over the depth of the column. The saturated and residual water contents are 0.287 and 0.075, respectively. The saturated hydraulic conductivity of the soil, K_s, is 0.34 m h^{-1}. The soil hydraulic property functions were presented by Haverkamp et al. (1977) as

$$S_w = \frac{A}{A + |h|^B} \tag{18a}$$

$$k_r(h) = \frac{C}{C + |h|^D} \tag{18b}$$

$$S_w = \frac{\theta - \theta_r}{\theta_s - \theta_r} \tag{18c}$$

where A, B, C and D are fitting parameters with the values of 1.616×10^6, 3.96, 1.18×10^6 and 4.74, respectively.

This problem was modelled as a 600 mm column. Solutions were obtained for each of two constant vertical grid spacings $\Delta y = 10$ and 25 mm, and for each of three time steps $\Delta t = 10$, 30 and 120 s. A dense grid solution with $\Delta y = 10$ mm and $\Delta t = 1$ s is considered to be the exact solution for this problem. The results of both mixed- and pressure-form approximations are demonstrated in Fig. 6. The value of R_{rms} for each case is given in Table 3 in which the better performance of the mixed-form formulation is clearly observed.

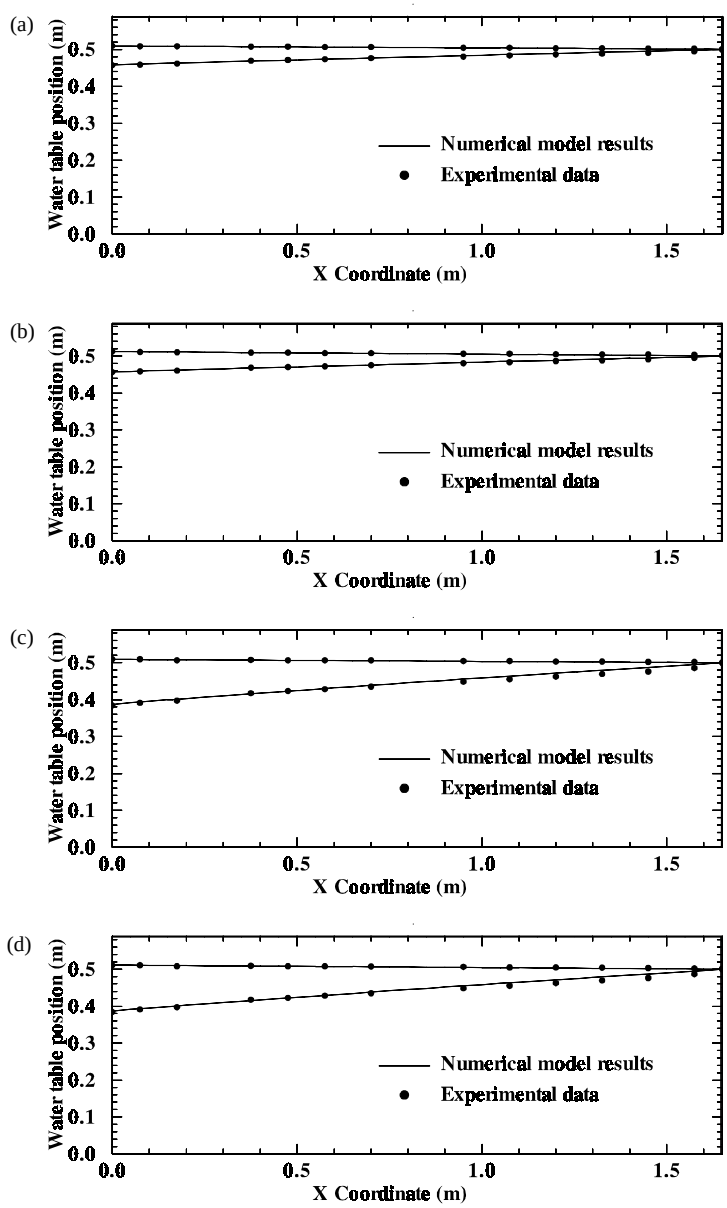

Fig. 11. Comparison of simulated and measured low and high water tables for data collected in experimental Run #: (a) 1; (b) 2; (c) 3; and (d) 4.

4.1.2. Case II: infiltration in a vertical soil column with pressure boundary condition

A constant head infiltration in a vertical column of soil is considered as the second example. This problem was simulated by Celia et al. (1990) and El-Kadi and Ling (1993). The column has a length of 1 m. The initial condition was set as a constant pressure head of -1 m, while the upper and lower boundary values were set at -750 mm and -1 m, respectively. The saturated hydraulic conductivity is 0.332 m h^{-1}, and the saturated and residual water content are, respectively, 0.368 and 0.102. The Van

Genuchten (1980) equations are used for unsaturated soil hydraulic properties,

$$S_w = \left[\frac{1}{1 + [\alpha|h|]^n} \right]^m \tag{19a}$$

$$k_r(S_w) = S_w^{(1/2)}[1-(1-S_w^{1/m})^m]^2 \tag{19b}$$

in which α, n and m are fitting parameters, with the values of 2.0 and 0.335 mm and with m related to n by $m = 1-(1/n)$.

The 1 m column of soil was discretised with two different vertical grid spacings $\Delta y = 10$, and 25 mm. Time steps were chosen equal to 20, 144 and 720 s. Fig. 7 shows the pressure head against depth for pressure- and mixed-form solutions. Table 4 gives the values of R_{rms} for these cases. The better accuracy of the mixed form solution is confirmed by visual inspection in Fig. 7 and by the R_{rms} comparison in Table 4. The improvement achieved through the mixed form of the equation is shown in Table 4 where, in general, the R_{rms} value for the pressure-form is an order of magnitude larger than the corresponding mixed-form value.

Based on Fig. 7 the results of the mixed-form solution are very close to the reference result for all cases, but the value of R_{rms} in some cases is larger than 0.10, which is the value proposed by Magnuson et al. (1990) as the upper limit of acceptability. For example, the values of R_{rms} for all cases with $\Delta y = 25$ mm are larger than 0.10 which was suggested by Magnuson et al. (1990) as the limit for acceptable accuracy. It appears that this R_{rms} upper limit may not be the most appropriate in cases when the moisture front is very sharp as in this example. Because a small amount of deviation from reference results causes a large value of R_{rms}, the graphical comparisons appear more useful in these cases.

4.2. Comparison with published results

In this section the ability of the numerical model to simulate the water table and seepage-face in 2D unconfined aquifers is assessed by modelling some examples for which published experimental data are available. The experimental results are those used by Zaradny (1993) and Clement et al. (1994) for the verification of their numerical models.

4.2.1. Case III: recharge to a water table in a 2D vertical sand slab; Vauclin et al. (1979)

The numerical model is checked by assessing its ability to duplicate the measured water table in a 2D experiment with infiltration to the top of soil stratum. The experiment was conducted in a laboratory on a slab of soil, 3 m long, 2 m high, and 0.05 m thick, by Vauclin et al. (1979). A constant flux corresponding to 0.148 m h^{-1} is applied over a width of 0.5 m. The water table was initially at a depth of 0.65 m, but the experiment was begun only after hydrostatic equilibrium had been established throughout the flow domain.

The sand was characterised by porosity $\varepsilon = 0.3$ and saturated hydraulic conductivity $K_s = 0.35$ m h^{-1}. The analytical expressions for the unsaturated hydraulic characteristics had the same form as Eqs. (18a)–(18c) with A, B, C and D equal to 4×10^4, 2.9, 2.99×10^6 and 5.0, respectively. Specific storage coefficient, S_s, was set to 10^{-4} m^{-1} for sand.

The nodal spacings in the horizontal and vertical directions are 0.2 and 0.1 m, respectively. The time step is varied from 5 to 300 s during simulation.

A comparison of calculated and measured water tables at $t = 2$, 3, 4 and 8 h is given in Fig. 8. The numerical model gives a very good prediction of water table location in this case.

4.2.2. Case IV: drainage from a 2D vertical sand slab; Vauclin et al. (1975)

The experimental data are used to examine the capability of the numerical model to simulate the water table in a 2D variably saturated flow with a seepage-face boundary. The experiment and its results are described in detail by Vauclin et al. (1975).

The physical set up is similar to the previous case, except that in this experiment the external water table is suddenly dropped from the height of 1.45 to 0.75 m at the start of the experiment.

The water retention of the sand and its relative hydraulic conductivity are described by Eqs. (18a)–(18c), using values of $A = 4 \times 10^4$, $B = 2.9$, $C = 3.6 \times 10^5$, $D = 4.5$, $\varepsilon = \theta_s = 0.3$ and $\theta_r = 0$. The saturated hydraulic conductivity is $K_s =$ 0.35 m h^{-1} and the specific storage coefficient, S_s, is assumed to be 10^{-4} m^{-1} for sand.

The nodal spacing in the horizontal and vertical

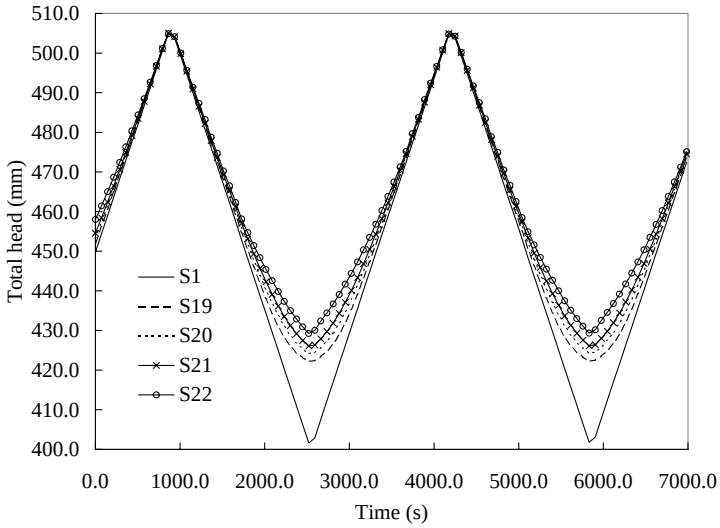

Fig. 12. Total pressure head at S1, S19, S20, S21 and S22 for Run #6.

directions are 0.2 and 0.1 m, respectively. The time step is varied from 5 to 300 s during simulation.

Fig. 9 illustrates the comparison of numerically simulated and measured water table positions at $t = 0.1$, 0.5, 1.0, 2.0, and 5.0 h. The numerical model has closely duplicated the experimental data.

4.3. Comparison with present experimental results

In this section the numerical model is verified against present experimental results. The ability of the numerical model to simulate the water table in the presence of periodic head boundary condition at the vertical face is verified using Run #1–4. Then the numerical model is applied to simulate the water table and the seepage-face for Run #5, which is a steady-state seepage through glass beads in the flow tank with a sloping face. Finally the numerical model is verified by the experimental results of Run #6 which is a case with a sloping face where a periodic head boundary condition applies.

4.3.1. Seepage through a 2D aquifer with a vertical face where a periodic head boundary condition is applied: Run #1–4

The present experimental data of Run #1–4 are used to examine the capability of the numerical model to simulate the water table in a 2D variably saturated flow with a periodic head boundary condition.

The water retention of the glass beads and its relative hydraulic conductivity are described by Eqs. (19a) and (19b), using values of: $\alpha = 8.6\ \mathrm{m}^{-1}$ and $n = 9.5$, $\varepsilon = \theta_s = 0.32$, and $\theta_r = 0.01$. The saturated hydraulic conductivity is $K_s = 15.42\ \mathrm{m\ h}^{-1}$ and the specific storage coefficient, S_s, is assumed to be $10^{-6}\ \mathrm{m}^{-1}$, which is almost corresponding to the compressibility of water. The boundary conditions at both ends of the flow tank were given in Table 2.

The nodal spacing in the horizontal and vertical directions are 2.5 and 5 cm, respectively. The time step is varied from 2.5 to 108 s during simulations.

Fig. 10 shows the total head at V1, V2, V4, V10, V11, V17 and V18 for experiment Run #3. As seen

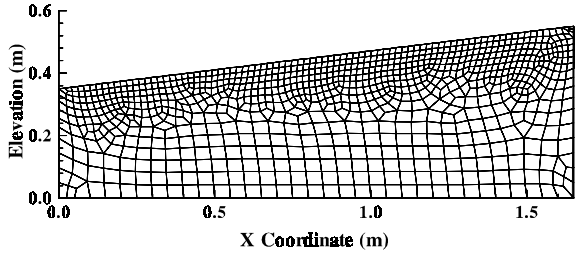

Fig. 13. Finite element mesh for simulation of experimental Run #5.

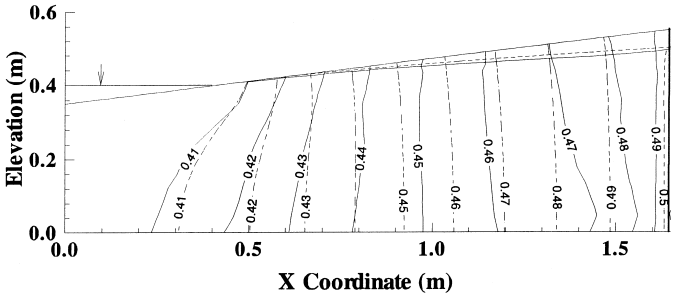

Fig. 14. Comparison of simulated (broken line) and measured (full line) water table and equipotential lines for Run #5.

there is no distinguishable difference between the total head for the tapping points with the same horizontal position but different elevations. This is observed for all experimental runs in the case of the aquifer with a vertical face. This observation indicates that no seepage-face exists in these cases, and therefore water level can be found directly from pressure readings.

Fig. 11 illustrates the comparison of numerically simulated and measured high- and low-water table positions for Run #1–4. The numerical model has closely duplicated the experimental data. Some discrepancies between the numerical and experimental results at the low water table condition are seen in Fig. 11(c) and (d) near the upstream reservoir. This is because of the loss in the hydraulic head at the upstream entrance as a result of the accumulation of air bubbles on the fine steel screen.

4.3.2. Seepage through a 2D aquifer with a sloping face

In both sets of experiments performed with a sloping faced aquifer for constant and periodic head boundary condition, a difference between the total head for the tapping points with same horizontal position but different elevations is observed. This observation indicates that a seepage face exists and/or vertical components of water flow velocities exist and are significant in these cases. Fig. 12 shows the total head at S1, S19, S20, S21 and S22 for experiment Run #6. The difference between the total heads is seen in this figure, especially when the water level at the periodic boundary is in the lowest position. Therefore the water table and equipotential lines for the constant and periodic boundary conditions are generated by interpolation based on the readings at pressure points using TECPLOT software.

4.3.3. Steady-state seepage through a 2D aquifer with a sloping face: Run #5

The data collected in Run #5 are used to examine the capability of the numerical model to simulate the water table and the seepage-face in a steady-state 2D variably saturated flow with a sloping face boundary. The slope is 1:8.25 and the other parameters are the same as for the previous case.

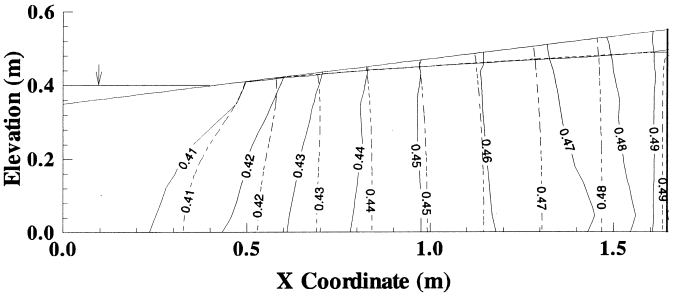

Fig. 15. Comparison of simulated (broken line), considering the effects of hydraulic loss at upstream, and measured (full line) water table and equipotential lines for Run #5.

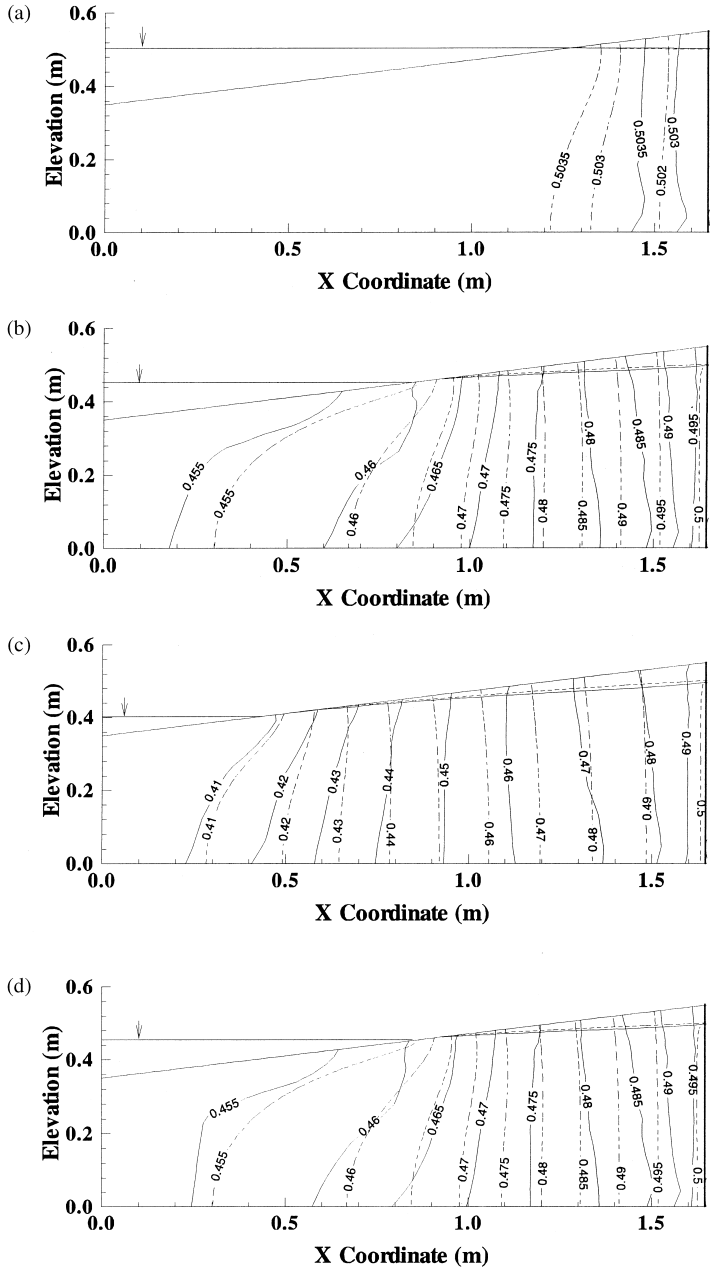

Fig. 16. Comparison of simulated (broken line) and observed (full line) corresponding to: (a) high; (b) falling; (c) low; and (d) rising water table and equipotential lines for Run #6.

The finite element mesh used for simulation is illustrated in Fig. 13. The element dimensions vary from 2 cm near the sloping part to 5 cm in the bottom part of the flow tank, and the number of nodes and elements are 980 and 906, respectively.

Water table and equipotential lines from numerical simulation (broken line) and measured data (solid

line) are shown in Fig. 14. Some differences between the results are seen at the up-stream end. The difference in the configuration between the observed and simulated equipotential lines at the upstream end might be because of heterogeneities in porous media due to packing or more likely due to non-uniform distribution of flux at the up-stream entrance because of the accumulation of air bubbles on the fine steel screen. Also, for the same reason, the loss of hydraulic head causes some discrepancies between the measured and simulated water table. However, in general the results match reasonably well, especially the water table and the seepage-face near the exit point, which are the major concerns in this verification test.

In order to show the effects of the hydraulic head loss at the up-stream boundary, the same problem is simulated by the numerical model for the case in which up-stream head is assumed to be 491 mm instead of 501 mm. Fig. 15 compares this numerical result with the measured one. In particular, the water tables are almost identical.

4.3.4. Seepage through a 2D sloping face aquifer with periodic head boundary condition: Run #6

The numerical model is tested by data collected in Run #6 to examine its capability to predict the water table and seepage-face in a 2D variably saturated flow with a sloping face and periodic head boundary condition. The mean water level at the downstream end is 453.5 mm and the amplitude and period of the linear periodic movement are 51.5 mm and 3300 s, respectively. The other physical and numerical parameters are the same as in the previous case.

The water table and equipotential lines for simulated (broken line) and observed (full line) data at different stages of water level fluctuation are shown in Fig. 16. As seen, the numerical model reproduces the measured data with adequate accuracy, particularly the water table and seepage-face near the sloping face, which are the most significant factors in this verification. As discussed in the previous section, the discrepancies between the results in the upstream part of flow tank can be explained by the effects of hydraulic head loss due to the accumulation of air bubbles.

5. Conclusions

A 2D numerical model for density dependent variably saturated groundwater flow was modified in order to be able to simulate the groundwater flow in unconfined aquifers affected by periodic boundary condition. The numerical model was verified against experimental data both published and obtained during this project. The influence of the form of the numerical approximation to the equation for variably saturated flow on the accuracy of the numerical solution and the improvement in results due to a change from pressure- to mixed-form were shown. Then, to examine the ability of the model to simulate 2D problems with complex boundary conditions, the numerical model is used to duplicate the results of some published experimental data for variably saturated problems. Physically measured data were produced for the groundwater response to a periodic boundary condition for aquifers with both vertical and sloping faces. Finally the numerical model successfully reproduced the present experimental results to confirm its capability of simulating complex boundary conditions like the periodic head and seepage face boundary condition on a sloping face.

Fluctuating the water table causes hysteresis in the vadose zone. This was not included in the code. Future work would include hysteresis effects in experimental measurements and numerical simulations.

Acknowledgements

The postgraduate scholarship of the Ministry of Culture and Higher Education of the Islamic Republic of Iran is appreciated. Financial assistance was provided partly by the Australian Research Council through a large grant for Coastal Groundwater Dynamics.

References

Ataie-Ashtiani, B., 1998. Contaminant transport in coastal aquifers. PhD Thesis, Department of Civil Engineering, University of Queensland, Australia.

Ataie-Ashtiani, B., Volker, R.E., Lockington, D.A., 1999. Tidal effects on sea water intrusion in unconfined aquifers. J. Hydrol. 216, 17–33.

Ataie-Ashtiani, B., Volker, R.E., Lockington, D.A., 1999. Contaminant transport in aquifers influenced by tide. Trans. Inst. Engnrs., Australia, Civil Engng, in press.

Celia, M.A., Bouloutas, E.T., Zarba, R.L., 1990. A general mass-conservative numerical solution for the unsaturated flow equation. Water Resour. Res. 26 (7), 1483–1496.

Clement, T.P., Wise, W.R., Molz, F.J., 1994. A physically based, two-dimensional, finite-difference algorithm for modelling variably saturated flow. J. Hydrol. 161, 71–90.

Cooley, R.L., 1971. A finite difference method for unsteady flow in variably saturated porous media: application to a single pumping well. Water Resour. Res. 7, 1607–1625.

Cooley, R.L., 1983. Some new procedures for numerical solution of variably saturated flow problems. Water Resour. Res. 19 (5), 1271–1285.

Demetriou, B.E., 1990. Effects of density contrasts on time-dependent mass transport in groundwater. PhD thesis, Department of Civil and Systems Engineering, James Cook University of North Queensland.

El-Kadi, A.I., Ling, G., 1993. The Courant and Peclet number criteria for the numerical solution of Richard's equation. Water Resour. Res. 29 (10), 3485–3494.

Fang, C.S., Wang, S.N., Harrison, W., 1972. Groundwater flow in a sandy tidal beach: two-dimensional finite element analysis. Water Resour. Res. 8, 121–128.

Haverkamp, R., Vauclin, M., Touma, J., Wierenga, P.J., Vachaud, G., 1977. Comparison of numerical simulation models for one-dimensional infiltration. Soil Sci. Soc. Am. J. 41, 13–20.

Huyakorn, P.S., Thomas, S.D., Thompson, B.M., 1984. Techniques for making finite elements competitive in modeling flow in variably saturated porous media. Water Resour. Res. 20 (8), 1099–1115.

Krikland, M.R., Hills, R.G., Wierenga, P.J., 1992. Algorithms for solving Richard's equation for variably saturated soils. Water Resour. Res. 28, 2049–2058.

Li, L., Barry, D.A., Pattiaratchi, C.B., 1997. Numerical modelling of tidal-induced beach water table fluctuations. Coastal Engng 30, 105–123.

Magnuson, S.O., Baca, R.G., Sondrup, A.J., 1990. Independent verification and benchmark testing of the PORFLO-3 computer code, version 1.0, Rep. EGG-BG-9175, Idaho Natl. Lab., Idaho Falls, Idaho, 1990.

Neuman, S.P., 1973. Saturated-unsaturated seepage by finite elements. J. Hydraul. Div. Am. Soc. Civil Engng. 99 (Hy12), 2233–2250.

Nielsen, P., 1990. Tidal dynamics of the watertable in beaches. Water Resour. Res. 26 (9), 2127–2134.

Oostrom, M., Hayworth, J.S., Dane, J.H., Guven, O., 1992. Behavior of dense aqueous phase leachate plumes in homogeneous porous media. Water Resour. Res. 28 (8), 2123–2134.

Philip, J.R., 1973. Periodic non-linear diffusion: an integral relation and its physical consequences. Aust. J. Phys. 26, 513–519.

Press, W.H., Flannery, B.P., Teukolsky, S.A., Vetterling, W.T., 1987. Numerical Recipes, Cambridge University Press, New York 818pp.

Rubin, J., 1968. Theoretical analysis of two-dimensional, transient flow of water in unsaturated and partly saturated soils. Soil Sci. Soc. Am. Proc. 32, 607–615.

Smiles, D.E., Stokes, A.N., 1976. Periodic solutions of a nonlinear diffusion equation used in groundwater flow theory: examination using a Hele–Shaw model. J. Hydraul. 31, 27–35.

Van Geel, P.J., Sykes, J.F., 1994. Laboratory and model simulations of a LNAPL spill in a variably saturated sand. 1. Laboratory experiment and image analysis techniques. J. Contam. Hydrol. 17, 1–25.

Van Genuchten, M.Th., 1980. A closed-form equation for predicting the hydraulic conductivity of unsaturated soils. Soil Soc. Am. J. 44, 892–898.

Vauclin, M., Vachaud, G., Khanji, J., 1975. Two-dimensional numerical analysis of transient water transfer in saturated-unsaturated soils. In: Vansteenkiste, G.C. (Ed.). Computer Simulation of Water Resources Systems, Proceedings of the IFIP Working Conference, North-Holland, Amsterdam, pp. 299–323.

Vauclin, M., Khanji, D., Vachaud, G., 1979. Experimental and numerical study of a transient, two-dimensional unsaturated-saturated water table recharge problem. Water Resour. Res. 15 (5), 1089–1101.

Volker, R.E., Ataie-Ashtiani, B., Lockington, D.A., 1997. Groundwater behaviour in tidal beaches. Proceedings of the 27th Congress of the International Association for Hydraulic Research, pp. 511–517.

Voss C.I., 1984. SUTRA: a finite element simulation model for saturated–unsaturated, fluid-density dependent ground-water flow with energy transport or chemically reactive single species solute transport. US Geological Survey, National Centre, Reston VA.

Waygal, R.J., 1963. Construction of models that simulate oil reservoirs. Soc. Pet. Engng. J., 281–286.

Zaradny, A., 1993. In: Zeidler, R.B. (Ed.). Groundwater Flow in Saturated and Unsaturated Soil, Balkema, Amsterdam.